

Influence of Edge Functionalization on Electronic and Optical Properties of Armchair Phosphorene Nanoribbons: a First-Principles Study

Pritam Bhattacharyya,^{1,*} Rupesh Chaudhari,¹ Naresh Alaal,^{2,†} Tushar Rana,³ and Alok Shukla^{1,‡}

¹*Department of Physics, Indian Institute of Technology Bombay, Powai, Mumbai 400076, India*

²*Physical Sciences and Engineering Division, King Abdullah University of Science and Technology, Thuwal 23955-6900, Saudi Arabia*

³*Department of Physics and Nanotechnology, SRM Institute of Science and Technology, SRM Nagar, Kattankulathur - 603203 (Tamil Nadu), India*

In this work, we present a systematic first-principles density-functional theory based study of geometry, electronic structure, and optical properties of armchair phosphorene nanoribbons (APNRs), with the aim of understanding the influence of edge passivation. Ribbons of width ranging from 0.33 nm to 3.8 nm were considered, with their edges functionalized with the groups H, OH, F, Cl, S, and Se. The geometries of various APNRs were optimized, and the stability was checked by calculating their formation energies. Using the relaxed geometries, calculations of their band structure and optical properties were performed. Pristine APNRs, as expected, exhibit significant edge reconstruction, rendering them indirect band gap semiconductors, except for one width ($N = 5$, where N is the width parameter) for which a direct band gap is observed. The edge passivated APNRs are found to be direct band gap semiconductors, with the band gap at the Γ -point, for all the functional groups considered in this work. To obtain accurate estimates of band gaps, calculations were also performed using HSE06 hybrid functional for several APNRs. Our calculations reveal that functional groups have significant influence on the band gaps and optical properties of narrower APNRs. For wider passivated ribbons, with the increasing ribbon widths, the gaps converge to almost the same value, irrespective of the group. We also performed calculations including the spin-orbit coupling (SOC) for hydrogen passivated APNRs with $N = 5$ and 11. We found that SOC has no significant influence on the band structure of the studied APNRs. However, for the broader APNR, a lowering of peak intensities was observed in the optical absorption spectrum beyond 5 eV.

I. INTRODUCTION

For the past few decades, there has been tremendous amount of interest in reduced-dimensional systems, in general, and two-dimensional (2D) materials, in particular.^{1–5} Not only are 2D materials interesting from the basic science point of view, they also offer easier tuning of their electronic properties, as compared to their bulk counterparts. The tailoring of their electronic properties is crucial to make them suitable for applications in electronics and optics. Phosphorene not only has a finite direct band gap, but also has high carrier mobility, and in-plane anisotropy. This 2D-material offers many potential applications not only in transport-based electronic and spintronic devices, but also in sensors, information storage, and optoelectronic devices.⁶ After the successful exfoliation of phosphorene from bulk black phosphorus,^{7–12} it has been a subject of extensive experimental as well as theoretical research.^{8,13–17} The band gap of phosphorene can be further tailored by manipulating the number of layers, in-layer strain,⁸ forming heterostructures such as nanoribbons and quantum dots, as well as by chemical means such as edge passivation.

In this work, we present a systematic first-principles density functional theory (DFT) based study of the geometry, electronic structure, and optical properties of armchair-type phosphorene nanoribbons (APNRs), with the aim of understanding the influence of edge-passivation on them. Numerous theoretical studies of phosphorene and its heterostructures have been performed over last few years, therefore, it is difficult to cite all of them. However, below we review the most relevant theoretical studies of the electronic structure and related properties of APNRs, which have been studied mainly using two methodologies: (a) semi-empirical tight-binding model, and (b) first-principles DFT.

Using the tight-binding model Sisakht and coworkers¹⁸ studied the scaling laws in phosphorene nanoribbons (PNRs), Soleimanikahnoj and Knezevic¹⁹ and Forte *et al.*²⁰ studied the effect of vertical electric field on electronic and transport properties of multilayer APNRs, while Yuan and Cheng²¹ investigated the influence of strain on the transport properties of APNRs.

Guo *et al.*²² studied the electronic structure and geometries of bare and H-passivated APNRs using a first-principles DFT based approach. Using the DFT²³ Tran and Yang studied the electronic structure and optical absorption of H-passivated APNRs, and also reported scaling laws for their band gaps. Carvalho and coworkers²⁴ computed the formation energies of APNRs, and also examined the edge-induced gap states in them, employing DFT and analytical models. The influence of edge-passivation by chemical groups such as H, F, Cl, O, S, Se, and OH, on the electronic properties of APNRs was studied by Peng *et al.*²⁵, using the DFT. Maity and coworkers²⁶ studied edge reconstruction and Peierls transition in PNRs, using a DFT based approach. Wu *et al.*²⁷ computed the electronic and transport properties of H-passivated APNRs using a methodology combining DFT and nonequilibrium Green's functions (NEGF.). The electronic structure and the Seebeck coefficients of H-passivated PNRs, with possible thermoelectric applications, were studied by Zhang *et al.*²⁸ also using the first-principles DFT. Hu, Lin, and Yang²⁹ studied the edge reconstruction in unpassivated PNRs, including a few thousands to ten thousand atoms in their calculations, by means of Discontinuous Galerkin DFT (DGDFT) methodology. The optical properties of relatively narrow APNRs were studied by Nourbakhsh and Asgari³⁰, by going beyond the first-principles DFT approach, by including electron-correlation and particle-hole effects within G_0W_0 and Bethe-Salpeter equation (BSE) methodology, including excitonic effects. Shekarforoush, Shiri and Khoeini³¹ computed the linear and non-linear optical properties of H-passivated APNRs of moderate widths, using first-principles DFT. Kaur *et al.*³² also employed the first-principles DFT to study the electronic, structural, and mechanical properties of PNRs of several allotropes of phosphorene. Electronic structure of pristine and APNRs passivated by H, O, and OH was studied by Ding and coworkers³³ using first-principles DFT. Possibility of using bilayer PNRs as pressure sensors was explored by Lv *et al.*³⁴ theoretically, using the first-principles DFT. Li and coworkers³⁵ also studied the electronic structure of both pristine and H-passivated PNRs of moderate widths, using the first-principles DFT. Using a similar computational approach, Gueorguiev and coworkers have studied other lower-dimensional systems, such as bismuth sheets, and carbon chains.^{36,37}

In this work, we have studied both the pristine and the passivated APNRs ranging from very narrow ribbons of width 0.32 nm to very broad ones of width 3.85 nm, using the PBE functional. The widths of nanoribbons can also be denoted using an integer parameter N (see Fig. 1(a)), in terms of which the APNRs studied in this work are in the range $3 \leq N \leq 24$. The novel aspects of this work are: (a) the maximum width of ribbons studied in this work is more than the earlier first-principles DFT based studies, such as H-passivated APNRs of maximum width 2.50 nm by Tran *et al.*²³, and pristine and passivated APNRs by Peng *et al.*²⁵, on selective widths up to 3.50 nm, (b) narrow pristine APNRs of widths $N = 3 - 5$ have been studied, for which no earlier work has been reported, (c) the optical absorption spectra of pristine and all edge-passivated APNRs, whereas the earlier calculations employing the same approach exist only for H-passivated ribbons,²³ (d) the bands involved in the transitions leading to a few important peaks in the absorption spectrum have been identified, (e) for obtaining more accurate estimates of the band gaps, we also performed the band structure calculations using the HSE06 hybrid functional for ribbons of medium width, with several passivating groups, whereas earlier calculations were performed only for -H, and -OH passivated ribbons.³³ Additionally, we also analyzed the calculated data of formation energies and concluded that: (i) the smaller ribbons

are more stable than the wider APNRs, (ii) F- and OH-saturated structures are comparatively much more stable, as compared to the H-passivated ones. Furthermore, we also performed a detailed analysis of the contributions of various atoms to the orbitals in the frontier regions of valence and conduction bands. To the best of our knowledge, none of the previous works has presented calculations on electronic and optical properties of APNRs over such a large range of width, for a variety of passivating groups.

The remaining part of this paper is organized as follows. The theoretical approach and technical details are described in the next section. We discuss and present our results in the section III. Finally, we present our conclusions in section IV.

II. THEORETICAL APPROACH AND COMPUTATIONAL DETAILS

The nanoribbons investigated in this work were taken to be periodic along the y -direction, with at least 15 Å vacuum included in the supercell along both the x - and z - directions to minimize the spurious interactions. First, geometry optimization for each ribbon was performed, followed by the calculations of quantities such as formation energies, the band gaps, the band structure, and the optical absorption spectra. The calculations were carried out by employing the first principles *ab initio* comprehensive density functional theory (DFT),³⁸ as implemented in the computer program Vienna Ab-initio Simulation Package (VASP).^{39,40} For the purpose, we used projector-augmented wave (PAW) pseudo-potentials^{41,42} and Perdew-Burke-Ernzerhof (PBE) exchange-correlation functional⁴³ for geometry optimization.

The kinetic energy cut-off of 500 eV was used for the plain wave basis set. For geometry optimization, a k-point grid of $1 \times 14 \times 1$ were chosen in the reciprocal space by employing Monkhorst-Pack centered at the Γ point. During geometry optimization, the convergence cutoff for the electronic energy was 10^{-5} eV, while that for Hellmann-Feynman force was set to 10^{-2} eV/Å. For subsequent total energy and density of states calculations, a tighter energy cutoff of 10^{-6} eV, along with a denser k-mesh grid of $1 \times 45 \times 1$, were employed. For band structure calculations of the optimized APNRs, 100 k-points were included for the path from Γ to Y. Both the PBE and Heyd-Scuseria-Ernzerhof (HSE06)⁴⁴ hybrid functionals were employed for self-consistent electronic structure calculations.

III. RESULTS AND DISCUSSION

In this section we present and discuss the results of our calculations on the geometry, stability, electronic structure, and optical properties of APNRs, with edges passivated by different functional groups.

A. Geometry

Henceforth, we denote a given ribbon by its width N (see Fig. 1(a)), thus an APNR of width N will be denoted as N -APNR. Additionally, edge bond angles and bond lengths relevant for both passivated and pristine nanoribbons are also defined in Fig. 1. We performed geometry optimization for N -APNRs, with $3 \leq N \leq 24$, for all functional groups except OH and F, for which we performed calculations only for $N = 11$. Optimized geometries for all functional groups as well for the pristine case are presented in Table I, for $N = 11$. Using the same methodology we performed geometry optimization on phosphorene monolayer for reference, and the corresponding relaxed geometry parameters are also presented in Table I. We note that our optimized geometries both for APNRs and phosphorene monolayer are in excellent agreement with results reported by Peng et al.²⁵, also based upon first-principles DFT.

For the pristine APNRs, the P-P bond length, l_2 has been reduced significantly as compared to the other structures in order to stabilize the dangling bonds at the edges, and, because of that, the bond angles α and θ have also increased considerably. Generally, one observes the tendency that larger the edge passivating atom/group, the longer the corresponding bond length. In the present case also the tendency holds true in that when selenium (Se) passivates the edge, l_3 is the longest as compared to its values for other edge atoms. As far as interior bond lengths and angles are concerned, they differ from their edge counterparts by small amounts.

B. Formation energy and relative stability

To quantify the energetic stability of an APNR, we define its formation energy (E_{form}) as follows

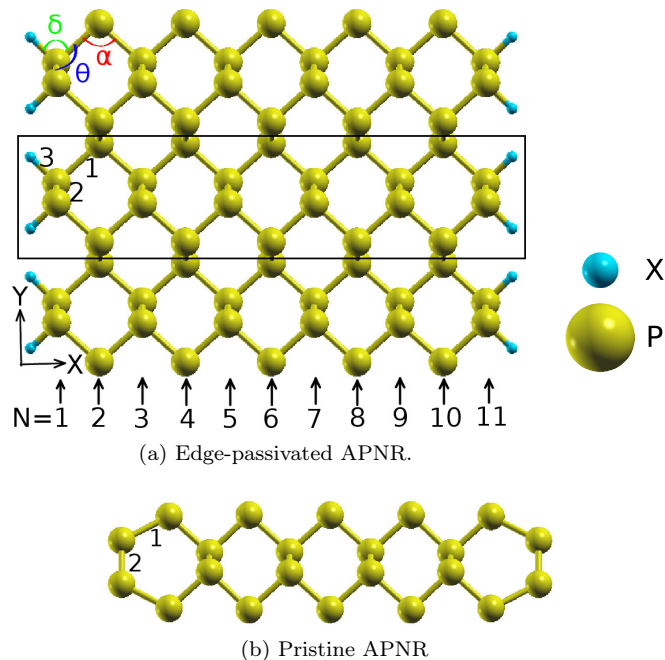


Figure 1: Relaxed geometry of 11-APNRs with and without edge passivation, where X denotes the passivating atom/group. 1, 2, and 3 indicate the bonds corresponding to the bond lengths l_1 , l_2 , and l_3 respectively, whose values are presented in Table I.

Table I: The bond lengths (l_1 , l_2 , l_3) and the bond angles (α , θ , δ) at the edges of the APNRs are shown in the Fig.1 where the bond lengths are denoted according to their subscript 1, 2 and 3.

| Structure | l_1 (Å) | l_2 (Å) | l_3 (Å) | α (°) | θ (°) | δ (°) |
|------------|--------------|--------------|--------------|-----------------|-----------------|-----------------|
| Mono-layer | 2.22 | 2.26 | NA | 95.9 | 104.1 | NA |
| Pristine | 2.23 | 2.07 | NA | 110.8 | 119.4 | NA |
| H | 2.22 | 2.25 | 1.44 | 95.9 | 103.3 | 93.0 |
| OH | 2.25 | 2.26 | 1.64 | 96.9 | 99.9 | 103.2 |
| F | 2.23 | 2.25 | 1.64 | 94.7 | 97.8 | 98.6 |
| Cl | 2.24 | 2.26 | 2.07 | 92.1 | 96.1 | 101.7 |
| S | 2.23 | 2.25 | 2.12 | 97.1 | 104.9 | 99.5 |
| Se | 2.23 | 2.24 | 2.28 | 95.3 | 102.9 | 100.0 |

$$E_{form} = E_{total} - N_p E_p - N_e E_e, \quad (1)$$

where E_{form} and E_{total} , respectively, are the formation energy and total energy of a pure or edge-passivated APNR within a super-cell containing N_p phosphorus atoms, and N_e passivation atoms/groups at the edge. Furthermore, E_p is the energy per phosphorus atom of an infinite phosphorene sheet, and E_e is the energy of a edge-passivating foreign atom which we calculated as $E_e = E_{e2}/2$. For the case of edge passivation by OH group, we used $E_e = (E_{O_2} + E_{H_2})/2$. Thus, the formation energy measures energetic stability of an edge-passivated APNR, with respect to an infinite phosphorene sheet. Negative value of E_{form} clearly implies that the formation of a given APNR from phosphorene sheet is energetically possible. In our calculations, $N_e=4$ for all APNRs considered in this work (see Fig. 1), while N_p depends on the width of the nanoribbon. For example, for 11-APNR, $N_p=22$. Energies of all the molecules considered as functional group are presented in the Table S1 of the supporting information. In the pristine case, the third term on the right hand side of Eq. 1 is absent. In Fig. 2a, we present the plot of the width dependence of the formation energy per phosphorus (P) atom (E_{form}/N_p) for all the pristine and edge-saturated APNR structures considered in this work, while the formation energies of pristine as well as edge-passivated 11-APNRs are plotted

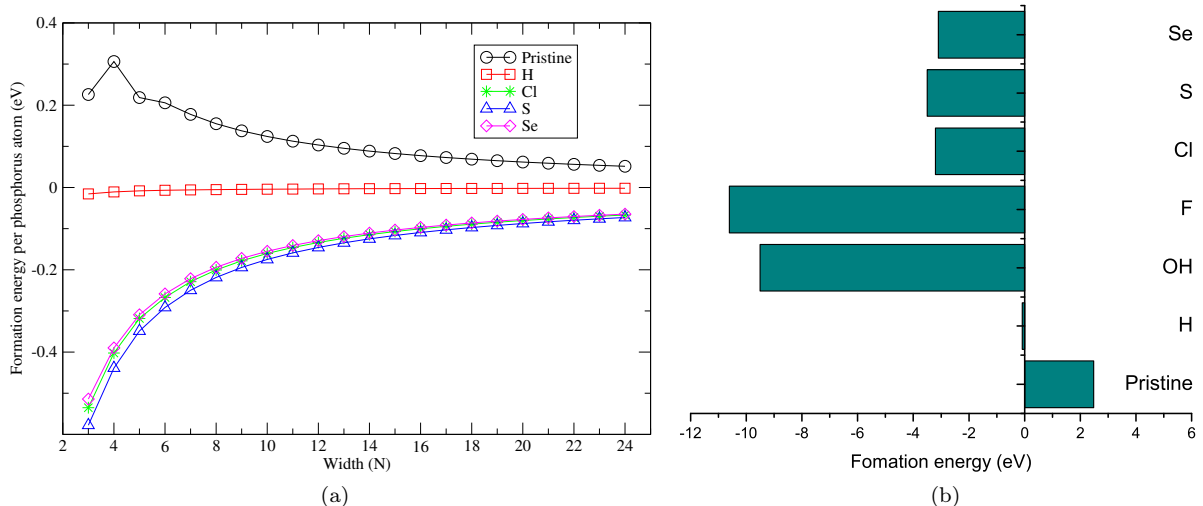


Figure 2: Formation energies of APNRs calculated using the PBE functional: (a) width dependence of formation energy per P-atom for pristine and various edge-saturated cases, and (b) formation energies of 11-APNRs, for various edge saturations.

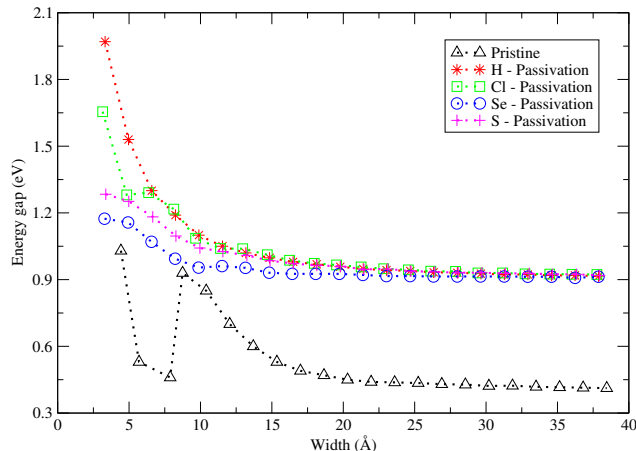


Figure 3: Variation of Band-gap of APNRs (up to 3.85 nm) with respect to the ribbon width.

in Fig. 2b. The following trends emerge from these figures: (a) with positive values of E_{form} , pristine APNRs are energetically unstable, however, their values of E_{form}/N_p are decreasing with the width, i.e., they are reaching the limit of infinite sheet, (b) for H-passivated ribbons, the formation energies are negative, but much smaller than those for APNRs passivated by other groups, (c) for all edge-passivated APNRs, the formation energy per P-atom is gradually increasing with the ribbon-width, and saturating for larger widths, implying that the narrower saturated ribbons are more stable than the broader ones. For the specific case of 11-APNR (see Fig. 2b), we note that the F-passivated APNR is most stable, closely followed by the OH passivated ribbon. These results of ours are consistent with those reported by Ding *et al.*³³.

C. Band gaps

In this section we discuss the band gaps of APNRs as functions of their width, and edge-passivating groups.

In Fig.3, we present the band gaps of APNRs as functions of their widths, and our results are in good agreement with those reported in earlier studies.^{23,25} An examination of the figure reveals the following general trends: (a) with the increasing width, the band gaps show a decreasing trend approaching saturation around 2.5 nm, (b) for a given width, the band gap of a pristine nanoribbon is smaller than that of a passivated one, and the difference grows with

Table II: Band gaps (in eV) of N -APNRs ($N = 3 - 9$), for various passivating atoms, calculated using the PBE functional.

| Passivating Atom | N | | | | | | |
|------------------|------|------|------|------|------|------|------|
| | 3 | 4 | 5 | 6 | 7 | 8 | 9 |
| H | 1.97 | 1.53 | 1.30 | 1.19 | 1.10 | 1.05 | 1.02 |
| Cl | 1.66 | 1.28 | 1.29 | 1.22 | 1.09 | 1.04 | 1.04 |
| S | 1.28 | 1.25 | 1.18 | 1.10 | 1.04 | 1.03 | 1.01 |
| Se | 1.17 | 1.16 | 1.07 | 0.99 | 0.95 | 0.96 | 0.95 |

Table III: Comparison of the band gaps of pristine and edge-saturated 11-APNRs computed using PBE and HSE06 hybrid functionals

| Structure | Band-gap (eV) | | Band-gap type |
|-----------|---------------|-------|---------------|
| | PBE | HSE06 | |
| Pristine | 0.49 | 1.05 | Indirect |
| H | 0.98 | 1.68 | direct |
| OH | 0.99 | 1.68 | direct |
| F | 0.96 | 1.65 | direct |
| Cl | 0.99 | 1.68 | direct |
| S | 0.97 | 1.67 | direct |
| Se | 0.92 | 1.64 | direct |

the increasing width, before eventually saturating, (c) for a given width, H-passivated ribbons have the largest band gaps, while those passivated with Se have the smallest. But for the pristine ribbons a peculiar behavior is observed in that the band gaps do not exhibit a monotonic decrease with increasing width, for narrower ribbons. At first, the band-gap decreases and reaches close to the final saturation value, then suddenly increases again, eventually exhibiting a normal decreasing trend with respect to the width. and follows the regular trend. This is mainly due to the huge distortion in the smaller structures to stabilize the dangling bonds which make changes in the symmetry of wave function of the edge states. To the best of our knowledge, so far there is no literature on on the electronic structure of pristine APNRs, with widths in the range $N = 3 - 5$.

It is also instructive to compare our obtained band gaps with that of infinite phosphorene monolayer. Using the PBE functional, and the geometry parameters listed in Table I, for the monolayer phosphorene we obtained the band gap to be 0.91 eV. This compares well with our saturated values of 0.92 eV for the H-passivated APNRs, and 0.91 for the selenium passivated ribbons. However, it is significantly larger than the saturated band gap value of 0.40 eV obtained for the pristine APNRs, thereby implying that pristine APNRs, due to their distorted edges, do not correctly evolve into monolayer phosphorene, with the increasing width. To examine the effect of spin-orbit coupling, we carried out calculations for hydrogen saturated 5- and 11-APNRs, but no significant changes were observed.

It is well-known that DFT-PBE based approaches generally underestimate the bang gaps significantly, therefore, one can wonder as to how reliable are our PBE functional based calculations, both quantitatively, and qualitatively. To verify that, we performed band gap calculations on 11-APNRs for pristine as well as various edge-passivated configurations using the HSE06 functional, and the results are presented in Table III, along with the corresponding values obtained using the PBE functional. HSE06 functional belongs to the class of hybrid functionals,^{45,46} whose predicted band gap values are normally fairly accurate, and compare well with the experiments.^{47,48} We note the following: (a) HSE06 band gap values for all the cases are significantly higher as compared to the PBE values, and (b) the trends in the band gap values ranging from pristine ribbons to the ones passivated by Se atom are similar for both the HSE06 and PBE calculations. Therefore, we conclude that although PBE functional significantly underestimates the band gaps, however it reproduces the qualitative features of the behavior of band gaps with respect to the passivation groups. Based upon these results, and the data presented in Fig. 3 and Table II, we can say with certainty that for the narrower APNRs, band gaps depend very sensitively on the nature of edge passivation; those passivated by H atoms have the largest gaps, while Se passivated ones have the smallest gaps. This information can be used to tune the electronic and optical properties of APNRs.

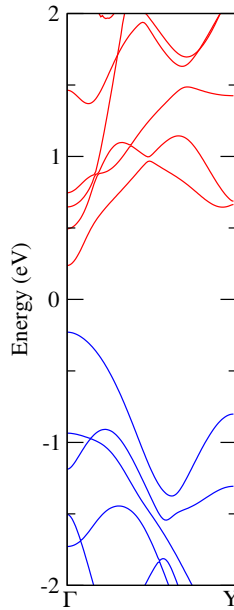


Figure 4: Band-structures of pristine 5-APNR

D. Band structure and density of states (DOS)

The computed band structures of pristine as well as passivated 11-APNR are shown in the Fig. 5. Our calculations reveal that the band gaps of pristine APNRs of all but one width are indirect, with the valence band maximum (VBM) at Γ point, and the conduction band minimum (CBM) between the Γ and Y points. The only exception to this is 5-APNR which, as shown in Fig. 4, is a semiconductor with a direct band gap of about 0.46 eV, at the Γ point. To the best of our knowledge, the band structure of pristine 5-APNR has not been discussed in the literature earlier, and the reasons behind its direct band gap could lie in its geometry, presented in Fig. S1 of the Supporting Information. The bond lengths l_1 and l_2 of 5-APNR are 2.30 Å and 2.29 Å, respectively, which are elongated with respect to the wider pristine structures. As far as bond angles are concerned, the calculated value of α is 121.4° , which is larger as compared to wider APNRs, while the value of θ at 110° is smaller as compared to the wider ribbons.

The passivated nanoribbons, irrespective of their width, or the nature of the passivating groups, turn out to be direct band gap semiconductors, with the VBMs and CBMs located at the high symmetry Γ point. This is obvious from the Fig. 5, which contains the band structures of 11-APNRs passivated by H, OH, F, Cl, S, and Se. These results of ours are in very good qualitative and quantitative agreement with the calculations of Peng *et al.*²⁵ and Tran and Yang²³. We performed calculations including the spin-orbit coupling for hydrogen passivated 5- and 11-APNRs, and observed no significant changes in the band structures.

For the edge-passivated APNRs, we find that both the VBM and the CBM derive predominant contributions from p-type orbitals of P atoms located both on the edges, as well as the interior of the ribbons. However, for the Se-passivated APNRs, the lowest conduction band, including the CBM, is mainly composed of the p-type orbitals located on the Se atoms. As far as deeper valence band orbitals are concerned, they derive dominant contribution from the s-type orbitals of the P atoms. The contributions of passivating atoms to two lowest conduction bands increase with the increasing atom sizes, being negligible for H-passivated ribbons, and eventually reaching maximum values for Se-passivated APNRs. A possible reason behind this behavior is that the electron clouds of larger passivating atoms are extended further into the interior of the nanoribbon, allowing its hybridization with the lower conduction bands leading to their lowering, thus causing a reduction in the band gaps.

We have compared the band structure of H-passivated 11-APNR computed using the HSE06 functional, with that obtained from the PBE functional, in Fig. S4 of the Supporting Information. The HSE06 band structure calculations were initiated using the PBE wave functions, and from the figure it is obvious that the HSE bands close to the Fermi level are similar to the PBE ones, except undergoing a rigid shift resulting from the widening of the band gap. Similar trends were also observed in the HSE band structures of APNRs passivated by other groups.

The total, orbital projected, and atom projected density of states (DOS) for the case of 11-APNRs are presented in Fig. 6. For the pristine ribbon, we note that the edge P atoms contribute more to the conduction band states near the Fermi level, as compared to the interior P atoms; while for the valence bands, both the interior as well edge atoms

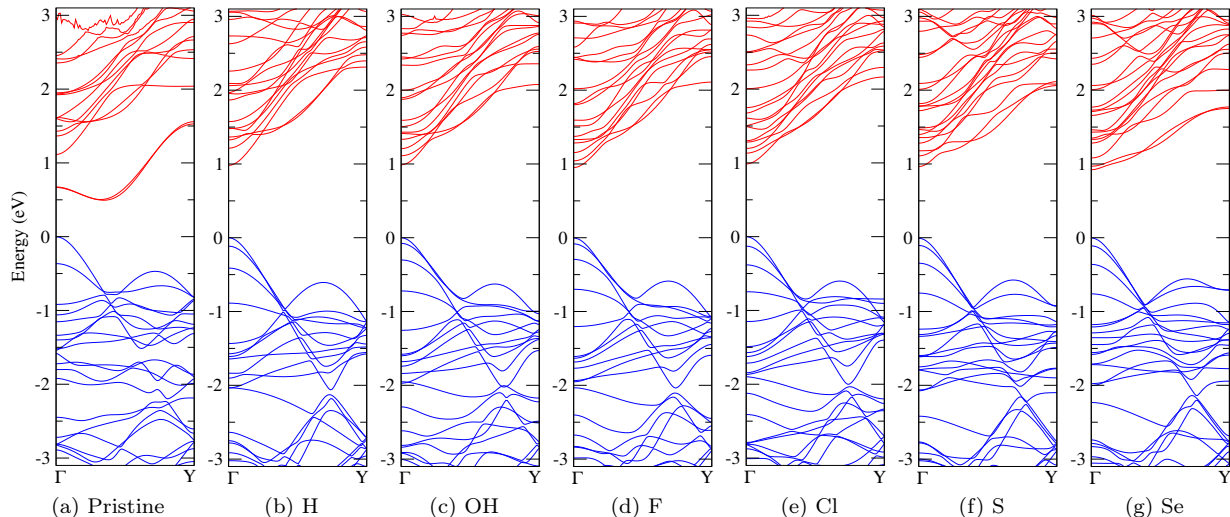


Figure 5: Band-structures of pristine and passivated 11-APNRs. The blue and red curves are the states corresponding to the valence and the conduction bands, respectively.

make significant contributions. For the passivated APNRs, we see that both the edge and the interior P atoms make significant contributions to the frontier bands. Furthermore, increasing contribution of the passivating atoms to the bands near the Fermi level, with their increasing sizes is also obvious from various DOS plots. It is also clear from these plots that the p-type orbitals contribute more than the s-type orbitals to the frontier states.

E. Optical absorption spectra

Based upon the single-particle DFT-PBE level band structure calculations, we computed the optical absorption spectra of pristine, as well as edge-saturated N-APNRs with various functional groups, for $N=3-24$, with the incident light polarized along the length of the ribbons. The spectrum was calculated according to the standard formalism, by computing the imaginary part of the dielectric constant matrix, as implemented in the VASP program.^{39,40}

In Fig. 7 we present the calculated optical absorption spectra of pristine and edge-passivated 11-APNRs. To the best of our knowledge, the only previous calculation of the absorption spectrum of APNRs, based upon the first-principles DFT methodology, was reported by Tran *et al.*²³, for H-passivated ribbons, but only up to 2.4 eV. Here we report calculations not just on H-passivated APNRs, but also on pristine ribbons, and also those passivated by other groups. In Fig. S3 of Supporting Information, we also present the results of similar calculations on narrower 5-APNRs, and broader 24-APNRs.

To investigate the effects of spin-orbit coupling (SOC) on the absorption spectra of APNRs, we carried out calculations for hydrogen passivated 5- and 11-APNRs, and in Fig. S6 of the Supporting Information, we compare the spectra computed with and without SOC. For the narrower ribbon, i.e., 5-APNR, no significant change in peak locations as well as intensity was observed. But, for the broader ribbon, i.e., 11-APNR, although no noticeable change in the peak locations is seen, but the peak intensities do get weaker for energies beyond 5 eV.

In order to benchmark the calculated spectra, in Table IV we compare the locations of our absorption peaks, with those reported by Tran *et al.*²³, for H-passivated ribbons. Because Tran *et al.*²³ reported the spectra only up to 2.4 eV, therefore, for $N=3$ and $N=5$, we are able to compare only one peak each, while for $N=10$, comparison for three peaks is possible (see Table IV). We note that the our peak locations are about 0.1 eV blue shifted as compared to the ones reported by Tran *et al.*²³, which is a fairly good agreement given the fact that they employed a different computer code, Quantum Espresso⁴⁹, for their calculations.

On examining the absorption spectra of 11-APNRs in Fig. 7, we see the following trends: (a) for the pristine ribbon there is no peak at the location of its band gap, consistent with the fact that it is an indirect band gap semiconductor, (b) for all the passivated ribbons, as expected, the first peak occurs at the location of the band gap, and (c) for all the APNRs, the highest intensity peak occurs at energies larger than 4 eV.

We present the locations of the first, the second, and the most intense peaks of optical absorption spectra of pristine and passivated 11-APNRs in the Table V. We also investigated the orbitals involved in the one-electron transitions leading to these peaks, and they are also presented in the same Table, in parentheses next to the peak energies. We

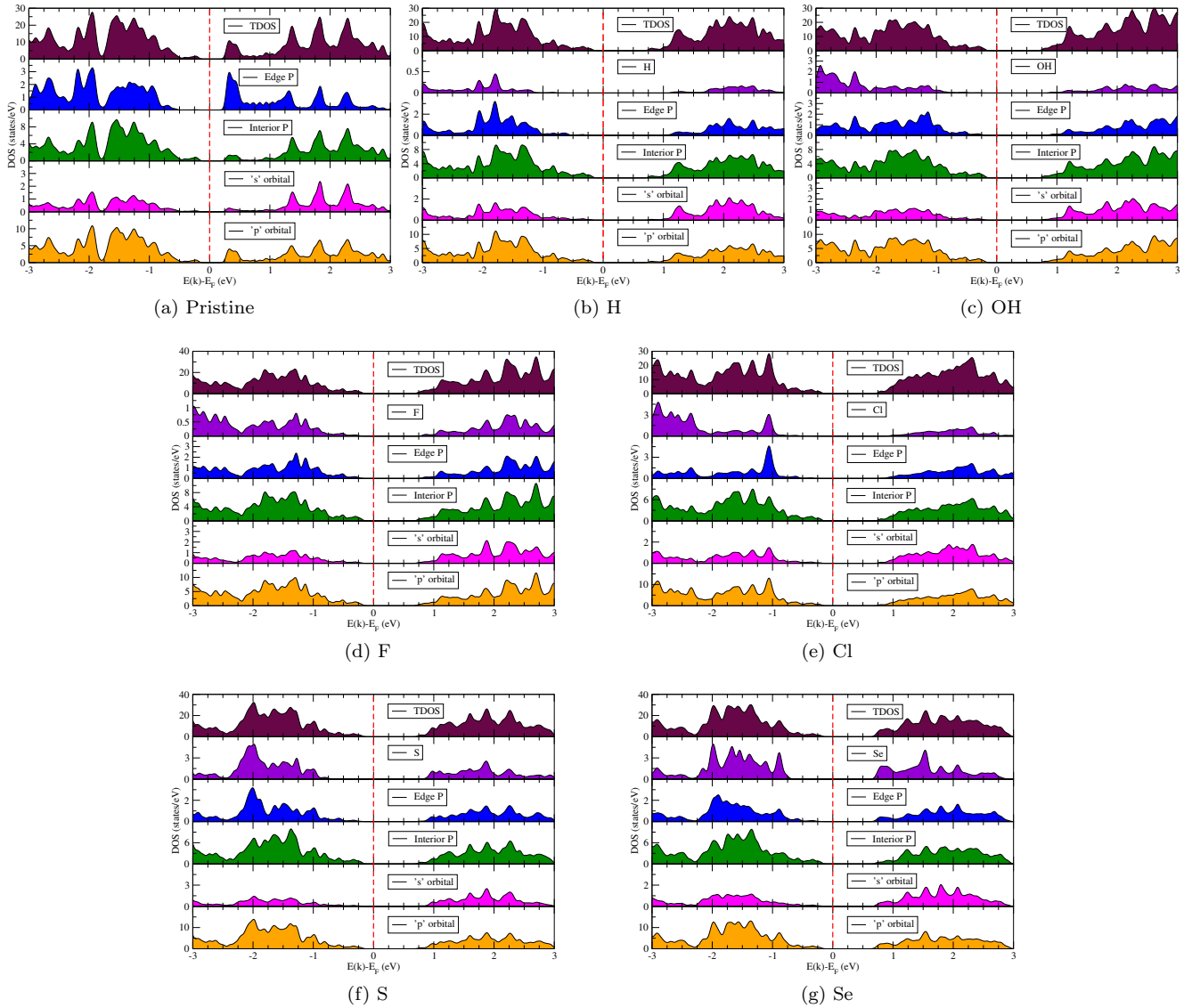


Figure 6: Total, atom projected, and orbital projected density of states (PDOS) of pristine and saturated 11-APNRs. The atom projected DOS is further classified based on the contributions from the passivating groups, as well as from P atoms located on the edges (“Edge P”), and the interior (“Interior P”) of the APNRs.

Table IV: Comparing the peak positions (in eV) in optical absorption spectra of hydrogen-saturated N-APNRs computed by us, with those reported by Tran and Yang²³. For N=10, first three peak locations are compared. Both the calculations are based on DFT-PBE formalism.

| N | This work | Tran et al.(Ref. ²³) |
|----|-----------|----------------------------------|
| 3 | 2.05 | 1.93 |
| 5 | 1.37 | 1.25 |
| 10 | 1.03 | 0.93 |
| | 1.49 | 1.4 |
| | 2.29 | 2.19 |

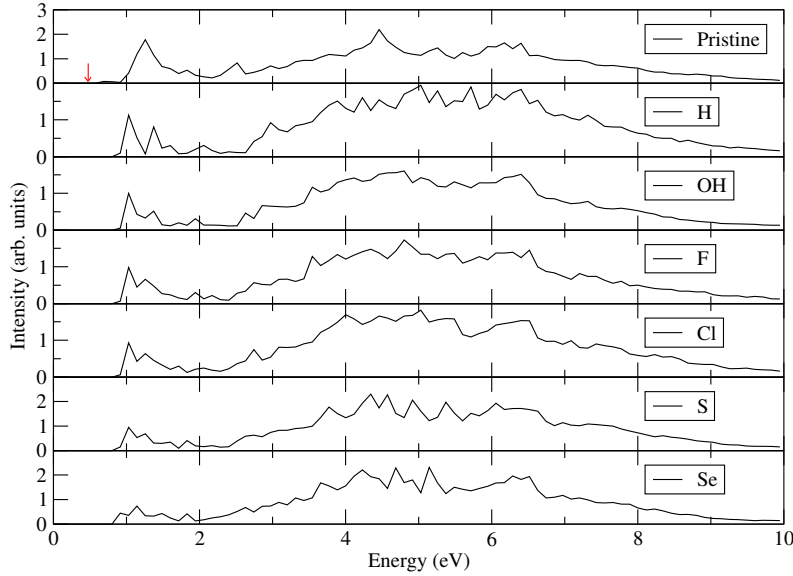


Figure 7: Single-particle optical absorption spectra of bare and edge-saturated 11-APNRs computed using DFT-PBE based formalism. The calculated band-gap is indicated by a red arrow for the pristine structure. In other cases the first peak position represents the band gap energy.

Table V: Locations of the first, second, and the most intense peaks, and the bands involved in the transition (in the parentheses), in the optical absorption spectra of pristine and saturated 11-APNRs. Below V and C denote the highest valance band, and the lowest conduction band, respectively. Similarly $V - n$ ($C + n$) denotes the n -th valence (conduction) band, counting away from the Fermi level.

| Saturation | First peak position (eV) | Second peak position (eV) | Most intense peak position (eV) |
|------------|--|--|--|
| Pristine | 0.69 ($ V \rightarrow C + 1\rangle$) | 1.26 ($ V \rightarrow C + 2\rangle$) | 4.46 ($ V - 8 \rightarrow C + 9\rangle$) |
| H | 1.03 ($ V \rightarrow C\rangle$) | 1.38 ($ V \rightarrow C + 3\rangle$) | 5.04 ($ V - 10 \rightarrow C + 10\rangle$) |
| OH | 1.03 ($ V \rightarrow C\rangle$) | 1.38 ($ V \rightarrow C + 3\rangle$) | 4.81 ($ V - 10 \rightarrow C + 8\rangle$) |
| F | 1.03 ($ V \rightarrow C\rangle$) | 1.28 ($ V \rightarrow C + 3\rangle$) | 4.82 ($ V - 10 \rightarrow C + 9\rangle$) |
| Cl | 1.03 ($ V \rightarrow C\rangle$) | 1.27 ($ V \rightarrow C + 3\rangle$) | 5.05 ($ V - 11 \rightarrow C + 12\rangle$) |
| S | 1.03 ($ V \rightarrow C\rangle$) | 1.27 ($ V - 1 \rightarrow C + 2\rangle$) | 4.35 ($ V - 8 \rightarrow C + 8\rangle$) |
| Se | 0.92 ($ V \rightarrow C\rangle$) | 1.14 ($ V \rightarrow C + 2\rangle$) | 5.16 ($ V - 14 \rightarrow C + 13\rangle$) |

note that for the pristine APNR, the first peak occurs at 0.69 eV, caused by the orbital transition $|V \rightarrow C + 1\rangle$, for a nonzero momentum value, very close to the Γ point. For all the passivated APNRs, the first peak appears due to the $|V \rightarrow C\rangle$ transition, occurring at the Γ point. The second peak for the pristine ribbon is due to the transition $|V \rightarrow C + 2\rangle$, slightly away from the Γ point. For APNRs passivated by monovalent groups, namely, H, OH, F and Cl, transition $|V \rightarrow C + 3\rangle$ gives rise to the second peak, while the same peak for the divalent passivating groups S and Se, is due to transitions $|V - 1 \rightarrow C + 2\rangle$, and $|V \rightarrow C + 2\rangle$, respectively. In all the cases, these optical transitions occur either at the Γ point, or fairly close to it. Finally, we examine the nature of the highest intensity peaks located at higher energies. Quite expectedly, the corresponding transitions involves bands far away from the Fermi level (see Table V), and they occur closer to the edge of the Brillouin zone, as shown for the case of H-saturated 11-APNR, in Fig. S2 of the Supporting Information.

At this point, one may wonder as to how close are the absorption spectra of our widest system 24-APNR to that of the infinite phosphorene monolayer. To investigate that, in Fig. S5 of the Supporting Information, we compare the optical absorption spectra of H-passivated 24-APNR to that of monolayer phosphorene, both computed using the DFT-PBE approach. From the figure it is obvious that the two spectra are very similar to each other in terms of intensity profile, as well as peak locations, except that the monolayer spectrum, quite expectedly, is much more intense. Thus, for all practical purposes we can assume that the optical properties of 24-APNR have saturated to the monolayer value.

When we compare the absorption spectra of 11-APNRs with those of 5-APNRs and 24-APNRs (see Fig. S3, Supporting Information) we note that for the pristine 5-APNR, the first absorption peak is at the band gap, because it is a direct band gap material. For the passivated nanoribbons, we note that the basic qualitative features of the absorption spectra are the same irrespective of the widths. For narrower ribbons the absorption peaks are sharper and well separated, while for broader ones they evolve into absorption bands.

We also note that the qualitative features of the absorption spectrum of H-passivated 5-APNR computed using the GW+BSE approach³⁰ are quite similar to that computed by us using the PBE-DFT approach, except, of course, for the peak locations.

IV. CONCLUSIONS

In this work, we presented results on first-principles DFT calculations on pristine and passivated N -APNRs, ranging from the very narrow ($N = 3$), to the very broad ($N = 24$). We first performed geometry optimization for each ribbon, and for those geometries computed quantities such as the formation energies, the band gaps, the band structure, and the optical absorption spectra, using the PBE functional. In addition, for a selected few ribbons, we also calculated the band gaps using the HSE06 functional, and found that it yields band gaps significantly larger than those predicted by PBE-functional based calculations. This implies that electron correlations make important contributions, highlighting their importance in the reduced dimensional systems such as APNRs. Therefore, by reducing the dimension of a system, one can manipulate the band gap as desired for a particular device application. Lower-dimensional materials can be useful in many applications such as sensors, information storage, optoelectronic devices, and transport and spintronic applications.

According to formation energy calculations, the pristine APNRs were predicted to be unstable, however, the results may change once the electron-correlation effects are taken into account. Formation energies also suggest that the narrower ribbons are more favorable than the wider ones, and that F- and OH-passivated ribbons are stabler as compared to other passivated ribbons.

Our calculations predict all pristine APNRs to be indirect band gap semiconductors, except for 5-APNR which was shown to have a direct band gap. Irrespective of the passivating group, all edge-saturated APNRs were found to be direct band gap materials, with the gap located at the Γ point. With the increasing width, band gaps of the passivated nanoribbons were shown to evolve to the band gaps of infinite monolayer phosphorene. However, pristine nanoribbons saturated to much smaller band gaps with increasing widths, indicating that the dangling bonds, and the related edge reconstruction, play important roles in their electronic properties.

To examine the influence of the relativistic effects, we also performed calculations on a couple of H-passivated APNRs including the spin-orbit coupling, and found no significant changes either in the band structure, or in the intensity profiles of the absorption spectra.

In this work we also presented a first-time systematic study of the dependence of optical absorption spectra on the passivating groups. We found that the first absorption peak corresponds to $V \rightarrow C$ excitation at the Γ point, corresponding to the band gaps, irrespective of the group. We also analyzed the bands involved in the higher energy transitions. As the self-energy corrections and excitonic effects were not incorporated in our calculations, detailed prediction of absorption profiles, which can be directly compared with the experiments, is not possible. It will, therefore, be interesting, in future, to perform calculations based upon GW-approximation and Bethe-Salpeter equations, to account for the influence of electron-correlation effects on the band structure and optical properties of wider APNRs.

AUTHOR INFORMATION

Corresponding Authors

Alok Shukla: *E-mail: shukla@phy.iitb.ac.in

Notes

The authors declare no competing financial interests.

ACKNOWLEDGEMENTS

Work of P.B. was supported by a Senior Research Fellowship offered by University Grants Commission, India. Also, we are thankful to the space-time server of IIT Bombay, India for providing computational facility to perform the calculations.

-
- * pritambhattacharyya01@gmail.com
† nareshkdnr@gmail.com
‡ shukla@phy.iitb.ac.in
- ¹ C. Cui, F. Xue, W.-J. Hu, and L.-J. Li, *npj 2D Materials and Applications* **2**, 18 (2018).
 - ² A. Carvalho, M. Wang, X. Zhu, A. S. Rodin, H. Su, and A. H. Castro Neto, *Nature Reviews Materials* **1**, 16061 (2016).
 - ³ M. Qiu, W. X. Ren, T. Jeong, M. Won, G. Y. Park, D. K. Sang, L.-P. Liu, H. Zhang, and J. S. Kim, *Chem. Soc. Rev.* **47**, 5588 (2018).
 - ⁴ M. Batmunkh, M. Bat-Erdene, and J. G. Shapter, *Advanced Materials* **28**, 8586 (2016), <https://onlinelibrary.wiley.com/doi/pdf/10.1002/adma.201602254>.
 - ⁵ D. Geng and H. Y. Yang, *Advanced Materials* **30**, 1800865 (2018), <https://onlinelibrary.wiley.com/doi/pdf/10.1002/adma.201800865>.
 - ⁶ M. Akhtar, G. Anderson, R. Zhao, A. Alruqi, J. E. Mroczkowska, G. Sumanasekera, and J. B. Jasinski, *npj 2D Materials and Applications* **1**, 5 (2017).
 - ⁷ L. Li, Y. Yu, G. J. Ye, Q. Ge, X. Ou, H. Wu, D. Feng, X. H. Chen, and Y. Zhang, *Nature Nanotechnology* **9**, 372 EP (2014), article.
 - ⁸ H. Liu, A. T. Neal, Z. Zhu, Z. Luo, X. Xu, D. Tománek, and P. D. Ye, *ACS Nano* **8**, 4033 (2014), pMID: 24655084, <https://doi.org/10.1021/nn501226z>.
 - ⁹ A. H. Woomer, T. W. Farnsworth, J. Hu, R. A. Wells, C. L. Donley, and S. C. Warren, *ACS Nano* **9**, 8869 (2015), pMID: 26256770, <https://doi.org/10.1021/acsnano.5b02599>.
 - ¹⁰ J. R. Brent, N. Savjani, E. A. Lewis, S. J. Haigh, D. J. Lewis, and P. O'Brien, *Chem. Commun.* **50**, 13338 (2014).
 - ¹¹ G. Zhinan, Z. Han, L. Shunbin, W. Zhiteng, T. Siying, S. Jundong, S. Zhengbo, X. Hanhan, W. Huaiyu, Y. Xue-Feng, and C. P. K., *Advanced Functional Materials* **25**, 6996 (2015).
 - ¹² A. Adriano, S. Zdenek, and P. Martin, *Angewandte Chemie International Edition* **56**, 10443 (2017), <https://onlinelibrary.wiley.com/doi/pdf/10.1002/anie.201705071>.
 - ¹³ L. Li, Y. Yu, G. J. Ye, Q. Ge, X. Ou, H. Wu, D. Feng, X. H. Chen, and Y. Zhang, *Nature Nanotechnology* **9**, 372 (2014).
 - ¹⁴ S. P. Koenig, R. A. Doganov, H. Schmidt, A. H. Castro Neto, and B. Ozyilmaz, *Applied Physics Letters* **104**, 103106 (2014), <https://doi.org/10.1063/1.4868132>.
 - ¹⁵ J. Dai and X. C. Zeng, *The Journal of Physical Chemistry Letters* **5**, 1289 (2014), pMID: 26274486, <https://doi.org/10.1021/jz500409m>.
 - ¹⁶ W. Zhu, M. N. Yogeesh, S. Yang, S. H. Aldave, J.-S. Kim, S. Sonde, L. Tao, N. Lu, and D. Akinwande, *Nano Letters* **15**, 1883 (2015), pMID: 25715122, <https://doi.org/10.1021/nl5047329>.
 - ¹⁷ W. Zhu, S. Park, M. N. Yogeesh, K. M. McNicholas, S. R. H. Bank, and D. Akinwande, *Nano Letters* **16**, 2301 (2016), pMID: 26977902, <https://doi.org/10.1021/acs.nanolett.5b04768>.
 - ¹⁸ E. Taghizadeh Sisakht, M. H. Zare, and F. Fazileh, *Phys. Rev. B* **91**, 085409 (2015).
 - ¹⁹ S. Soleimanikahnoj and I. Knezevic, *Journal of Computational Electronics* **16**, 568 (2017).
 - ²⁰ J. D. Forte, D. J. [de Sousa], and J. M. Pereira, *Physica E: Low-dimensional Systems and Nanostructures* **114**, 113578 (2019).
 - ²¹ Y. Yuan and F. Cheng, *AIP Advances* **7**, 075310 (2017), <https://doi.org/10.1063/1.4991494>.
 - ²² H. Guo, N. Lu, J. Dai, X. Wu, and X. C. Zeng, *The Journal of Physical Chemistry C* **118**, 14051 (2014), <https://doi.org/10.1021/jp505257g>.
 - ²³ V. Tran and L. Yang, *Phys. Rev. B* **89**, 245407 (2014).
 - ²⁴ A. Carvalho, A. S. Rodin, and A. H. C. Neto, *EPL (Europhysics Letters)* **108**, 47005 (2014).
 - ²⁵ X. Peng, A. Copple, and Q. Wei, *Journal of Applied Physics* **116**, 144301 (2014), <https://doi.org/10.1063/1.4897461>.
 - ²⁶ A. Maity, A. Singh, and P. Sen, "Peierls transition and edge reconstruction in phosphorene nanoribbons," (2014), arXiv:1404.2469.
 - ²⁷ Q. Wu, L. Shen, M. Yang, Y. Cai, Z. Huang, and Y. P. Feng, *Phys. Rev. B* **92**, 035436 (2015).
 - ²⁸ J. Zhang, H. J. Liu, L. Cheng, J. Wei, J. H. Liang, D. D. Fan, J. Shi, X. F. Tang, and Q. J. Zhang, *Scientific Reports* **4**, 6452 (2014), article.
 - ²⁹ W. Hu, L. Lin, and C. Yang, *Phys. Chem. Chem. Phys.* **17**, 31397 (2015).
 - ³⁰ Z. Nourbakhsh and R. Asgari, *Phys. Rev. B* **94**, 035437 (2016).
 - ³¹ S. Shekarforoush, D. Shiri, and F. Khoeini, *Journal of Applied Physics* **123**, 245113 (2018), <https://doi.org/10.1063/1.5029547>.
 - ³² S. Kaur, A. Kumar, S. Srivastava, R. Pandey, and K. Tankeshwar, *Nanotechnology* **29**, 155701 (2018).
 - ³³ B. Ding, W. Chen, Z. Tang, and J. Zhang, *The Journal of Physical Chemistry C* **120**, 2149 (2016), <https://doi.org/10.1021/acs.jpcc.5b09159>.

- ³⁴ Y. Lv, Q. Huang, S. Chang, H. Wang, and J. He, *IEEE Electron Device Letters* **38**, 1313 (2017).
- ³⁵ W. Li, G. Zhang, and Y.-W. Zhang, *The Journal of Physical Chemistry C* **118**, 22368 (2014), <https://doi.org/10.1021/jp506996a>.
- ³⁶ R. B. dos Santos, R. Rivelino, F. d. B. Mota, and G. K. Gueorguiev, *Phys. Rev. B* **84**, 075417 (2011).
- ³⁷ R. R. Q. Freitas, F. de Brito Mota, R. Rivelino, C. M. C. de Castilho, A. Kakanakova-Georgieva, and G. K. Gueorguiev, *Nanotechnology* **27**, 055704 (2016).
- ³⁸ W. Kohn and L. J. Sham, *Phys. Rev.* **140**, A1133 (1965).
- ³⁹ G. Kresse and J. Furthmüller, *Phys. Rev. B* **54**, 11169 (1996).
- ⁴⁰ G. Kresse and J. Furthmüller, *Computational Materials Science* **6**, 15 (1996).
- ⁴¹ P. E. Blöchl, *Phys. Rev. B* **50**, 17953 (1994).
- ⁴² G. Kresse and D. Joubert, *Phys. Rev. B* **59**, 1758 (1999).
- ⁴³ J. P. Perdew, K. Burke, and M. Ernzerhof, *Phys. Rev. Lett.* **77**, 3865 (1996).
- ⁴⁴ J. Heyd, G. E. Scuseria, and M. Ernzerhof, *The Journal of Chemical Physics* **118**, 8207 (2003), <https://doi.org/10.1063/1.1564060>.
- ⁴⁵ J. Heyd, G. E. Scuseria, and M. Ernzerhof, *The Journal of Chemical Physics* **118**, 8207 (2003), <https://doi.org/10.1063/1.1564060>.
- ⁴⁶ L. Schimka, J. Harl, and G. Kresse, *The Journal of Chemical Physics* **134**, 024116 (2011), <https://doi.org/10.1063/1.3524336>.
- ⁴⁷ R. R. Pela, M. Marques, and L. K. Teles, *Journal of Physics: Condensed Matter* **27**, 505502 (2015).
- ⁴⁸ A. J. Garza and G. E. Scuseria, *The Journal of Physical Chemistry Letters* **7**, 4165 (2016), <https://doi.org/10.1021/acs.jpcllett.6b01807>.
- ⁴⁹ P. Giannozzi, S. Baroni, N. Bonini, M. Calandra, R. Car, C. Cavazzoni, D. Ceresoli, G. L. Chiarotti, M. Cococcioni, I. Dabo, A. D. Corso, S. de Gironcoli, S. Fabris, G. Fratesi, R. Gebauer, U. Gerstmann, C. Gougoussis, A. Kokalj, M. Lazzeri, L. Martin-Samos, N. Marzari, F. Mauri, R. Mazzarello, S. Paolini, A. Pasquarello, L. Paulatto, C. Sbraccia, S. Scandolo, G. Sclauzero, A. P. Seitsonen, A. Smogunov, P. Umari, and R. M. Wentzcovitch, *Journal of Physics: Condensed Matter* **21**, 395502 (2009).

Supporting Information
Influence of Edge Functionalization on Electronic and Optical Properties of Armchair Phosphorene Nanoribbons: a First-Principles Study

Pritam Bhattacharyya,^{1,*} Rupesh Chaudhari,¹ Naresh Alaal,^{2,†} Tushar Rana,³ and Alok Shukla^{1,‡}

¹*Department of Physics, Indian Institute of Technology Bombay, Powai, Mumbai 400076, India*

²*Physical Sciences and Engineering Division, King Abdullah University of Science and Technology, Thuwal 23955-6900, Saudi Arabia*

³*Department of Physics and Nanotechnology, SRM Institute of Science and Technology, SRM Nagar, Kattankulathur - 603203 (Tamil Nadu), India*

Table S1: Total energies of the molecules computed using the PBE functional used for computing the formation energies of passivated APNRs

| Molecule | Energy (eV) |
|-----------------|-------------|
| H ₂ | -6.7009 |
| O ₂ | -9.8611 |
| F ₂ | -3.5524 |
| Cl ₂ | -3.5559 |
| S ₂ | -6.5951 |
| Se ₂ | -5.4183 |

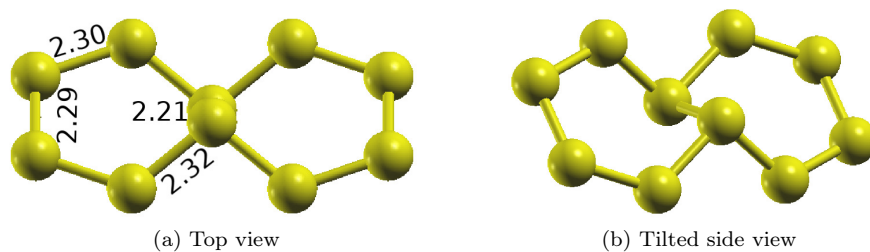


Figure S1: Optimized geometry of pristine 5-APNR

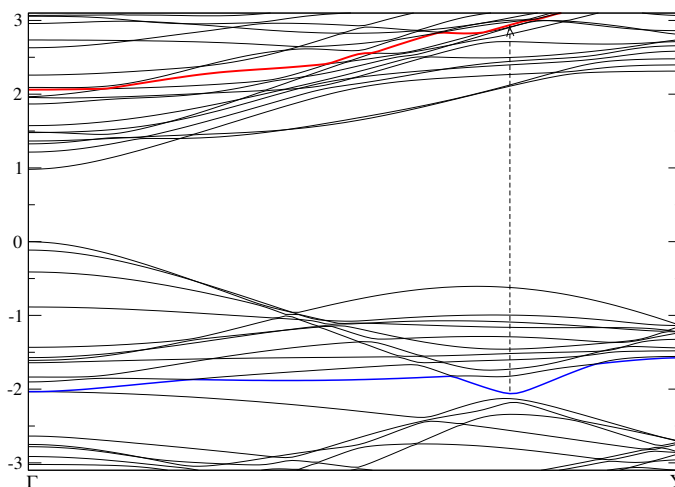


Figure S2: The arrow indicates the k value, as well as the involved bands, corresponding to the direct transition responsible for the most intense peak in the optical absorption spectrum of H-saturated 11-APNR. The involved valence and conduction bands are in blue and red colors, respectively.

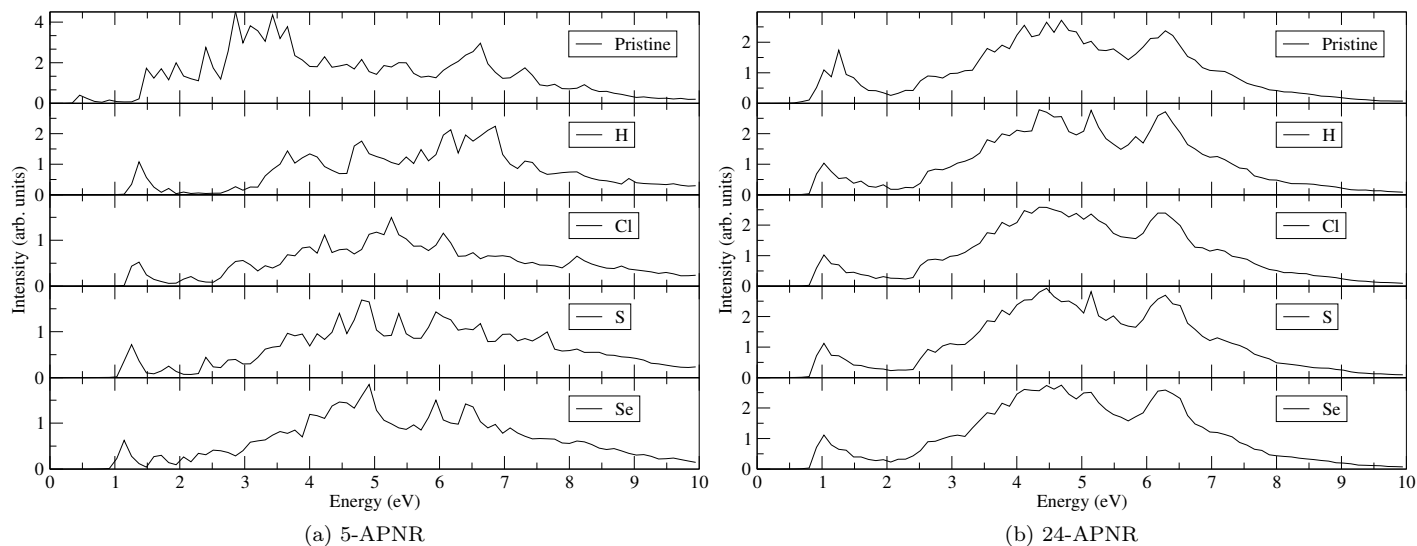


Figure S3: Optical absorption spectra of bare and saturated 5- and 24-APNR computed using the DFT-PBE methodology. In the pristine case of 5-APNR, the first peak of the optical spectrum is due to the transition at the band edge.

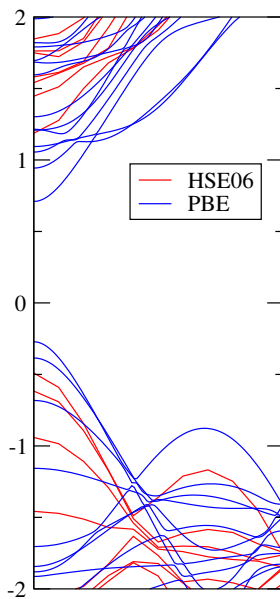


Figure S4: Comparison of band structures of hydrogen(H)-saturated 11-APNR, computed using the PBE and HSE06 hybrid functionals.

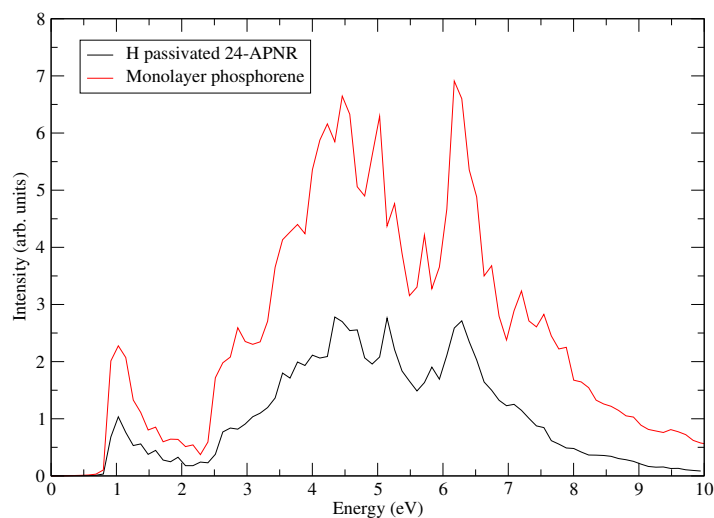


Figure S5: Optical absorption spectra of monolayer phosphorene compared to that of hydrogen-passivated 24-APNR, computed using the DFT-PBE methodology. Two spectra are very similar to each other except for larger intensity for the infinite monolayer.

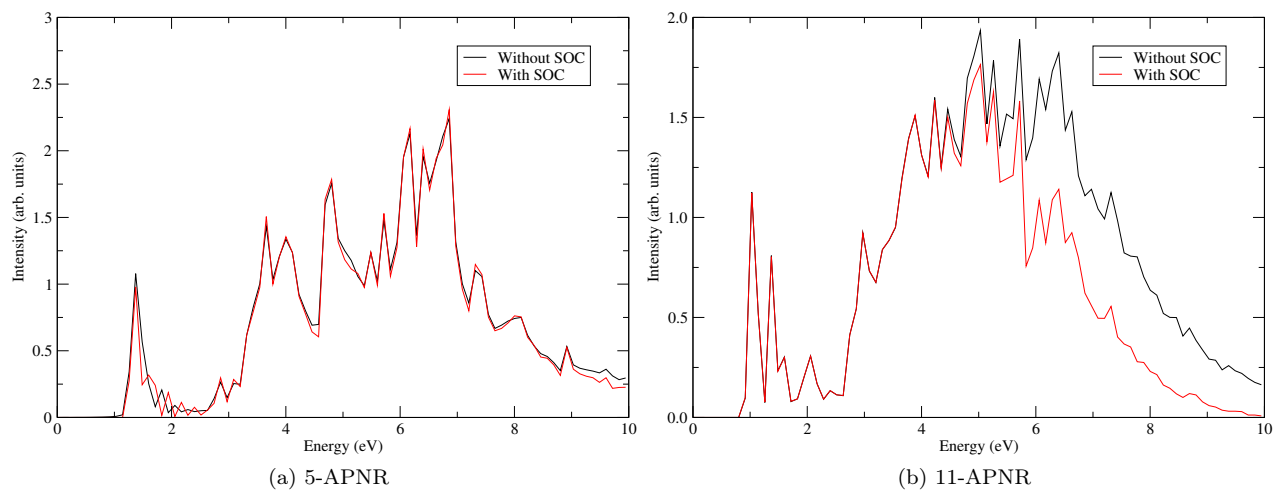


Figure S6: Optical absorption spectra of hydrogen-passivated (a) 5-APNR and (b) 11-APNR, without and with including the spin-orbit coupling (SOC), computed using the DFT-PBE methodology.